Optimal interpolation schemes for particle tracking in turbulence

M. A. T. van Hinsberg,[1,*] J. H. M. ten Thije Boonkkamp,[2] F. Toschi,[1,2,3] and H. J. H. Clercx[1,4,†]

[1]*Department of Physics, Eindhoven University of Technology, PO Box 513, 5600MB Eindhoven, The Netherlands*

[2]*Department of Mathematics and Computer Science, Eindhoven University of Technology, PO Box 513, 5600MB Eindhoven, The Netherlands*

[3]*CNR, Istituto per le Applicazioni del Calcolo, Via dei Taurini 19, 00185 Rome, Italy*

[4]*Department of Applied Mathematics, University of Twente, PO Box 217, 7500 AE Enschede, The Netherlands*

(Received 19 November 2012; published 15 April 2013)

An important aspect in numerical simulations of particle-laden turbulent flows is the interpolation of the flow field needed for the computation of the Lagrangian trajectories. The accuracy of the interpolation method has direct consequences for the acceleration spectrum of the fluid particles and is therefore also important for the correct evaluation of the hydrodynamic forces for almost neutrally buoyant particles, common in many environmental applications. In order to systematically choose the optimal tradeoff between interpolation accuracy and computational cost we focus on comparing errors: the interpolation error is compared with the discretization error of the flow field. In this way one can prevent unnecessary computations and still retain the accuracy of the turbulent flow simulation. From the analysis a practical method is proposed that enables direct estimation of the interpolation and discretization error from the energy spectrum. The theory is validated by means of direct numerical simulations (DNS) of homogeneous, isotropic turbulence using a spectral code, where the trajectories of fluid tracers are computed using several interpolation methods. We show that *B*-spline interpolation has the best accuracy given the computational cost. Finally, the optimal interpolation order for the different methods is shown as a function of the resolution of the DNS simulation.

DOI: 10.1103/PhysRevE.87.043307 PACS number(s): 47.11.Kb, 02.60.Ed, 02.60.Pn

I. INTRODUCTION

Pseudospectral codes in combination with accurate interpolation methods for particle tracking are commonly used in many applications [1–7]. The spectral code solves the flow field by means of direct numerical simulations in an Eulerian approach, while the particle trajectories are obtained by a Lagrangian approach. To compute the particle trajectories the fluid velocity must be known at the particle positions. The standard way to do this is by representing the Eulerian fluid velocity on a uniform, rectangular grid and make use of appropriate interpolation schemes to evaluate fluid velocities out of the grid. Many interpolation methods have been used, from low-order linear schemes [4] to high-order splines [5–7]. Because the interpolation step is time consuming and memory demanding, it is important to choose the best interpolation method for a given application. In order to get more accurate results the order of the interpolation method can be increased. Because high-order methods are computationally expensive, it is important to make the best tradeoff between accuracy and computational costs. The best tradeoff can be determined by using good error estimates, assuring that the high-order methods will give significantly more accurate results.

In many applications, and notably those where almost neutrally buoyant particles are involved, not only the fluid velocity is needed but also its first derivatives. The evaluation of these derivatives can also be computed efficiently by the interpolation method, by taking the derivative of the interpolating function [8]. A good approximation of the first derivative requires accurate interpolation methods. For the computation of the trajectories of (almost neutrally buoyant) particles we consider the equation discussed by Maxey and Riley [9], for small isolated rigid spherical particles ($d_p \ll \eta$, with d_p the particle diameter and η the Kolmogorov length scale) in a nonuniform velocity field $\mathbf{u}(\mathbf{x},t)$. An important assumption is that the particle Reynolds number is small, $\mathrm{Re}_p = d_p|\mathbf{u} - \mathbf{u}_p|/\nu \ll 1$, with $\mathbf{u}_p$ the velocity of the particle and ν the kinematic viscosity of the fluid. Because we consider small particle diameters and small particle volume fractions, we ignore the effects of two-way and four-way coupling. An overview of the different terms in the Maxey-Riley (MR) equation and its numerical implementation can be found in the paper by Loth [10] and a historical account of the equation of motion in a review article by Michaelides [11]. Time integration of the MR equation to compute particle trajectories can be an expensive, time- and memory consuming job, particularly for what concerns the computation of the Basset history force. However, a significant reduction in computational costs can be obtained by fitting the diffusive kernel of the Basset history force with exponential functions, as shown by van Hinsberg *et al.* [12].

A systematic way to determine the best tradeoff between interpolation accuracy and computational cost for a particular application is to compare errors: the interpolation error is compared with the discretization error of the flow field. In this way one can prevent unnecessary accurate and expensive computations. We will introduce different practical methods for computing these errors, and will investigate the following interpolation methods: Lagrange interpolation, spline interpolation, Hermite interpolation, and *B*-spline interpolation. For Hermite interpolation we use the method suggested by Choi *et al.* [13] who employed Hermite interpolation on multiple spatial points. For the *B*-spline interpolation the method of Van Hinsberg *et al.* [8] is used. These methods are also used in many other applications, including the computation of charged particles in a magnetic field [14,15], but also digital

*M.A.T.v.Hinsberg@tue.nl

†H.J.H.Clercx@tue.nl

filtering and applications in medical imaging [16,17]. In the latter case interpolations are used to improve image resolution. Besides the optimization of interpolation algorithms (accuracy, efficiency), the impact of different interpolation methods on physical phenomena, like particle transport, has been investigated in many studies [13,18–23]. To our knowledge, the direct comparison between the interpolation and the discretization error to make an optimal choise for the interpolation method has not yet been systematized; here we will give fundamental insight into this problem.

The theory is deduced for passive tracer particles because they are uniformly distributed in homogeneous isotropic turbulent flows, one of the hypotheses used in this study. For the application areas we have in mind, such as almost neutrally buoyant particles in environmental flows, hardly any preferential concentration is anticipated and a uniform distribution of the particles can safely be assumed. Therefore, also for this case all the hypotheses still hold and it is particularly interesting as the equation of motion of these particles contain acceleration derivatives which are often notoriously difficult to evaluate accurately with interpolation methods.

The manuscript is arranged as follows. Sections II and III give practical methods on how to estimate the interpolation error. Section II focuses on calculating the interpolation error offline. In this way only statistics of the turbulent flow are needed without having to compute interpolations. In Sec. III an even more practical method is proposed. This method only needs the energy spectrum to predict the interpolation error. A practical method for estimating the discretization error is discussed in Sec. IV. Next, the different interpolation methods employed are explained in Sec. V. Thereafter, the results of a comparison are shown in Sec. VI, where we give a prediction of the optimal order of the interpolation methods provided the spatial resolution of the smallest (turbulent) flow scale is known. Finally, concluding remarks are given in Sec. VII.

II. INTERPOLATION ERROR

This section focuses on the *a priori* estimation of the interpolation error. In this way only the statistics of the turbulent flow is needed without having to compute interpolations, an efficient method for estimating the interpolation error.

In general, the particle will follow a path $\mathbf{x}_p(t)$ and the flow velocity field is given by $\mathbf{u}(\mathbf{x},t)$. Suppose that we need to find the velocity at the particle position, i.e., $\mathbf{u}[\mathbf{x}_p(t),t]$, but instead we find the approximation $\widetilde{\mathbf{u}}[\mathbf{x}_p(t),t]$, due to the interpolation errors. Let $\mathcal{I}$ be the interpolation operator that maps $\mathbf{u}$ onto $\widetilde{\mathbf{u}}$, so $\widetilde{\mathbf{u}} = \mathcal{I}[\mathbf{u}]$. The relative interpolation error ϵ for one particle can be computed by the L^2-norm like

$$\epsilon = \lim_{T\to\infty} \frac{\|\mathbf{u}[\mathbf{x}_p(t),t] - \widetilde{\mathbf{u}}[\mathbf{x}_p(t),t]\|_T}{\|\mathbf{u}[\mathbf{x}_p(t),t]\|_T}, \tag{1}$$

where the time-averaging norm, $\|\cdot\|_T^2$, is given by

$$\|\mathbf{f}\|_T^2 = \frac{1}{T}\int_0^T |\mathbf{f}(t)|^2 dt, \tag{2}$$

and $|\cdot|$ denotes the usual 2-norm. Analogous to this, the norm is also used for scalar quantities. The value of $\mathbf{u}[\mathbf{x}_p(t),t]$ in relation (1) can be calculated from the Fourier components of the Eulerian flow field [obtained from the direct numerical simulations (DNS)], which is computationally expensive. Therefore, relation (1) will only be used to validate the following steps towards a more pragmatic approach to estimate the interpolation error.

We assume that the system is ergodic which means that the ensemble average is equal to the time average; therefore, ϵ does not depend on the choice of the particle and an average over particles can be taken. Furthermore, we assume that the particle has no preferential location and thus we can replace the particle average by a space average. We can thus average over space and time; in practice the time average needs to be performed over several large-eddy turnover times. The space average is taken over the whole domain V which is $[0,1)^3$ in dimensionless units. Notice that in order to simplify the notation we have chosen $[0,1)^3$ instead of the usual $[0,2\pi)^3$. In this way one can write ϵ like

$$\epsilon = \frac{\|\|\mathbf{u} - \widetilde{\mathbf{u}}\|_3\|_T}{\|\|\mathbf{u}\|_3\|_T}, \tag{3}$$

where we introduce the following inner products:

$$\begin{aligned}\langle \mathbf{f},\mathbf{g}\rangle_1 &= \int_0^1 (\mathbf{f}\cdot\mathbf{g}^*)(x)dx,\\ \langle \mathbf{f},\mathbf{g}\rangle_3 &= \int_0^1\int_0^1\int_0^1 (\mathbf{f}\cdot\mathbf{g}^*)(\mathbf{x})dx\,dy\,dz,\end{aligned} \tag{4}$$

and the corresponding norms:

$$\begin{aligned}\|\mathbf{f}\|_1^2 &= \langle \mathbf{f},\mathbf{f}\rangle_1 = \int_0^1 |\mathbf{f}(x)|^2 dx,\\ \|\mathbf{f}\|_3^2 &= \langle \mathbf{f},\mathbf{f}\rangle_3 = \int_0^1\int_0^1\int_0^1 |\mathbf{f}(\mathbf{x})|^2 dx\,dy\,dz.\end{aligned} \tag{5}$$

Here $\mathbf{f}\cdot\mathbf{g}$ denotes the usual inner product and $\mathbf{g}^*$ denotes the complex conjugate of $\mathbf{g}$. These inner products and norms are also used for scalar fields like f and g, where the inner product is reduced to the ordinary product fg^*. The velocity field is approximated in a three-dimensional Fourier series, like

$$\mathbf{u}(\mathbf{x},t) = \sum_{\mathbf{k}\in\mathbf{K}} \mathbf{u}_\mathbf{k}(t)\phi_\mathbf{k}(\mathbf{x}), \quad \phi_\mathbf{k}(\mathbf{x}) = e^{2\pi i\mathbf{k}\cdot\mathbf{x}}, \tag{6}$$

where $\mathbf{K}$ is the space of wave vectors $\mathbf{k}$, with $\mathbf{k} = (k_x,k_y,k_z)$ and $|\mathbf{k}| \leqslant k_{\max}$ the maximal wave number. We neglect the error made by taking a finite sum, which is a part of the discretization error (and should for a well-resolved simulation decrease exponentially in case of increasing resolution). The complex-valued functions $\phi_\mathbf{k}$ constitute an orthonormal basis with respect to the inner product $\langle\cdot,\cdot\rangle_3$. Introducing the interpolant of $\phi_\mathbf{k}$, $\widetilde{\phi}_\mathbf{k} = \mathcal{I}[\phi_\mathbf{k}]$, when the interpolation operator $\mathcal{I}$ is linear, one obtains

$$\epsilon = \frac{\|\|\sum_{\mathbf{k}\in\mathbf{K}} \mathbf{u}_\mathbf{k}(\phi_\mathbf{k} - \widetilde{\phi}_\mathbf{k})\|_3\|_T}{\|\|\sum_{\mathbf{k}\in\mathbf{K}} \mathbf{u}_\mathbf{k}\phi_\mathbf{k}\|_3\|_T}. \tag{7}$$

It can be proven, see [8], that $\phi_\mathbf{k} - \widetilde{\phi}_\mathbf{k}$ constitute an orthogonal basis with respect to the inner product $\langle\cdot,\cdot\rangle_3$ and we define $\gamma_\mathbf{k} = \|\phi_\mathbf{k} - \widetilde{\phi}_\mathbf{k}\|_3$. In this case we obtain

$$\epsilon = \frac{\|(\sum_{\mathbf{k}\in\mathbf{K}} \gamma_\mathbf{k}^2|\mathbf{u}_\mathbf{k}|^2)^{1/2}\|_T}{\|(\sum_{\mathbf{k}\in\mathbf{K}} |\mathbf{u}_\mathbf{k}|^2)^{1/2}\|_T}. \tag{8}$$

Changing the order of the norms gives

$$\epsilon = \frac{\left(\sum_{\mathbf{k}\in\mathbf{K}} \gamma_{\mathbf{k}}^2 \|\mathbf{u}_{\mathbf{k}}\|_T^2\right)^{1/2}}{\left(\sum_{\mathbf{k}\in\mathbf{K}} \|\mathbf{u}_{\mathbf{k}}\|_T^2\right)^{1/2}}. \tag{9}$$

Now ϵ can be calculated without having to do a simulation for all the interpolation methods, only $\|\mathbf{u}_{\mathbf{k}}\|_T$ is needed from the simulations. Next, we require $\mathcal{I}$ to satisfy

$$\begin{aligned}\tilde{\phi}_{\mathbf{k}} &= \mathcal{I}[\phi_{\mathbf{k}}] = \mathcal{I}[\phi_{k_x}\phi_{k_y}\phi_{k_z}] \\ &= \mathcal{I}_1[\phi_{k_x}]\mathcal{I}_1[\phi_{k_y}]\mathcal{I}_1[\phi_{k_z}] = \tilde{\phi}_{k_x}\tilde{\phi}_{k_y}\tilde{\phi}_{k_z},\end{aligned} \tag{10}$$

with $\mathcal{I}_1[\cdot]$ the one-dimensional variant of the operator $\mathcal{I}[\cdot]$. Using this property and $\|\phi_k\|_1 = 1$, $\gamma_{\mathbf{k}}^2$ can be written as

$$\gamma_{\mathbf{k}}^2 = 1 + s_1(k_x)s_1(k_y)s_1(k_z) - 2s_2(k_x)s_2(k_y)s_2(k_z), \tag{11}$$

with

$$s_1(k) = \|\widetilde{\phi}_k\|_1^2, \quad s_2(k) = \mathcal{R}(\langle\widetilde{\phi}_k,\phi_k\rangle_1), \tag{12}$$

with $\mathcal{R}(f)$ denoting the real part of f. Here, s_1 and s_2 can be calculated fast using methods from van Hinsberg *et al.* [8]. Now combining (9) with (11) and (12) gives us a method for the calculation of the interpolation error.

This method is based on the assumptions that there is no preferential position for the particles, an approach that is correct for fluid tracers in incompressible flows. Inertial particles will instead cluster depending on their size and density. The advantage of this method over using relation (1) is that no simulations of particle trajectories in turbulence have to be done when $\|\mathbf{u}_{\mathbf{k}}\|_T$ is known; the statistical information on the turbulent flow field itself is sufficient.

III. APPROXIMATION OF THE INTERPOLATION ERROR

In this section the error estimate ϵ is further simplified. In Eq. (9) a summation must be taken over all three-dimensional vectors $\mathbf{k} \in \mathbf{K}$. In order to evaluate only a one-dimensional sum one can use the assumption of statistical isotropy of the turbulent flow. In the end this results in a practical method that only needs the energy spectrum to predict the interpolation error.

Starting from Eq. (9), the summation is split as

$$\epsilon^2 = \frac{\sum_{k=0}^{k_{\max}} \sum_{\mathbf{k}\in\mathbf{K}_k} \gamma_{\mathbf{k}}^2 \|\mathbf{u}_{\mathbf{k}}\|_T^2}{\sum_{k=0}^{k_{\max}} \sum_{\mathbf{k}\in\mathbf{K}_k} \|\mathbf{u}_{\mathbf{k}}\|_T^2}, \tag{13}$$

where $\mathbf{K}_k$ is a subset of $\mathbf{K}$ which include $\mathbf{k}$ with $k - \frac{1}{2} \leqslant |\mathbf{k}| < k + \frac{1}{2}$. Next, the approximation is made that $\mathbf{K}_k$ includes $4\pi k^2$ wave vectors (the surface of a sphere with radius k). Assuming statistical isotropy the three-dimensional energy spectrum is spherically symmetric, and we can write $\|\mathbf{u}_{\mathbf{k}}\|_T = \|\mathbf{u}_k\|_T$ for $k = |\mathbf{k}|$ with $\mathbf{u}_k = \mathbf{u}_{\mathbf{k}}$ for $\mathbf{k} = (k,0,0)$. Using both assumptions (13) can be approximated with

$$\epsilon_{\text{iso}}^2 = \frac{\sum_{k=0}^{k_{\max}} k^2 \gamma_k^2 \|\mathbf{u}_k\|_T^2}{\sum_{k=0}^{k_{\max}} k^2 \|\mathbf{u}_k\|_T^2}, \quad \gamma_k^2 = \left[\gamma_{\mathbf{k}}^2\right]_{|\mathbf{k}|=k}, \tag{14}$$

where $[\cdot]_{|\mathbf{k}|=k}$ denotes the space average over the surface of a sphere in k space with radius k. Note that $(k\|\mathbf{u}_k\|_T)^2$ is proportional to the energy of the modes with $k = |\mathbf{k}|$. In this way the integrated energy spectrum in combination with γ_k is sufficient to calculate the error.

In order to be able to compute $[\gamma_{\mathbf{k}}^2]_{|\mathbf{k}|=k}$ easily, the following derivation is made. Starting from $\gamma_{\mathbf{k}} = \|\phi_{\mathbf{k}} - \widetilde{\phi}_{\mathbf{k}}\|_3$ and introducing $e_k = \phi_k - \widetilde{\phi}_k$, one finds

$$\gamma_{\mathbf{k}}^2 = \|\phi_{k_x}\phi_{k_y}\phi_{k_z} - (\phi_{k_x} - e_{k_x})(\phi_{k_y} - e_{k_y})(\phi_{k_z} - e_{k_z})\|_3^2. \tag{15}$$

We assume that the error is relatively small compared to the actual Fourier component. Under this assumption we have that $\|e_k\|_1 \ll \|\phi_k\|_1 = 1$ and only the lowest powers of e_k need to be taken into account. Using that $\|\phi_k\|_1 = 1$, one obtains

$$\begin{aligned}\gamma_{\mathbf{k}}^2 &\approx \|e_{k_x}\phi_{k_y}\phi_{k_z} + \phi_{k_x}e_{k_y}\phi_{k_z} + \phi_{k_x}\phi_{k_y}e_{k_z}\|_3^2 \\ &\approx \|e_{k_x}\|_1^2 + \|e_{k_y}\|_1^2 + \|e_{k_z}\|_1^2.\end{aligned} \tag{16}$$

In the last step we neglected the cross terms. We checked that the final contribution of the cross terms in the summation in relation (14) is only of the order of 5%; this is due to the fact that these terms mainly average out as they can be both positive and negative.

We restrict ourselves to polynomial interpolations and we define the order n of the method as follows: n is the highest degree of a polynomial for which the interpolation is still exact. When the order of the interpolation method is known the following approximation can be made:

$$\|e_k\|_1^2 \approx ck^{2(n+1)}, \tag{17}$$

where c is some constant. The reason for this formula is the following. Given that a method has order n the amplitude of e_k is proportional to the $(n+1)$th derivative of ϕ_k. From this, one gets that e_k is proportional to k^{n+1}. (This is also shown by Fig. 1 in Sec. VI.) Using this one finds that

$$\gamma_{\mathbf{k}}^2 \approx ck_x^{2(n+1)} + ck_y^{2(n+1)} + ck_z^{2(n+1)}. \tag{18}$$

Next, the average needs to be taken over a spherical surface, $[\gamma_{\mathbf{k}}^2]_{|\mathbf{k}|=k}$. Because of symmetry reasons we only need to calculate the contribution of $ck_z^{2(n+1)}$; the contributions of the other terms are equal to this one. The calculation for the surface average is done in spherical coordinates

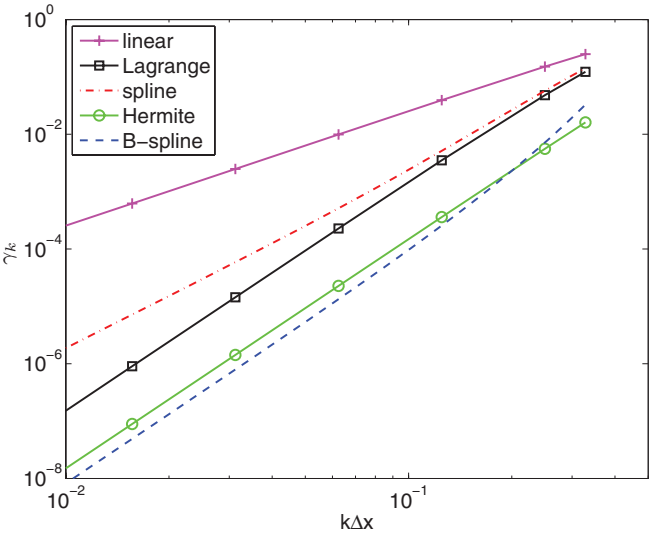

FIG. 1. (Color online) Interpolation error γ_k (20) of the various methods, calculated with the methods of van Hinsberg *et al.* [8]. For all methods $N = 4$ except for linear interpolation, which has $N = 2$.

$\mathbf{k} = k(\sin\varphi\ \cos\theta, \sin\varphi\ \sin\theta, \cos\varphi)$ as follows:

$$\begin{aligned}\frac{1}{3}\left[\gamma_{\mathbf{k}}^2\right]_{|\mathbf{k}|=k} &\approx c\left[k_z^{2(n+1)}\right]_{k=|\mathbf{k}|} \\ &= \frac{c}{4\pi k^2}\int_0^{\pi}\int_0^{2\pi}(k\ \cos\varphi)^{2(n+1)}k^2\sin\varphi\,d\theta\,d\varphi \\ &= \frac{ck^{2(n+1)}}{4\pi}\int_0^{\pi}\int_0^{2\pi}\cos^{2(n+1)}\varphi\ \sin\varphi\,d\theta\,d\varphi \\ &= \frac{ck^{2(n+1)}}{2n+3}. \end{aligned} \tag{19}$$

Thus we obtain

$$\gamma_k^2 = \left[\gamma_{\mathbf{k}}^2\right]_{|\mathbf{k}|=k} \approx \frac{3}{2n+3}ck^{2(n+1)} \approx \frac{3}{2n+3}\|e_k\|_1^2. \tag{20}$$

Combining Eq. (14) with (20) results in a practical method that only needs the energy spectrum to predict the interpolation error. Note that some approximations as discussed are needed and therefore the result will be somewhat less accurate than the expression derived in the previous section.

IV. DISCRETIZATION ERROR

As we will compare the interpolation error with the Eulerian discretization error $\bar{\delta}$, we take the same norm for both of them. A first suggestion would be

$$\bar{\delta} = \frac{\|\|\mathbf{u} - \widehat{\mathbf{u}}\|_3\|_T}{\|\|\widehat{\mathbf{u}}\|_3\|_T}, \tag{21}$$

where $\widehat{\mathbf{u}}$ is the exact Eulerian velocity field. In practice, what we call the "exact" velocity field is obtained by using double grid resolution. Expanding $\mathbf{u}$ and $\widehat{\mathbf{u}}$ in a Fourier series gives

$$\bar{\delta} = \frac{\|\|\sum_{\mathbf{k}\in\mathbf{K}}\mathbf{u}_{\mathbf{k}}\phi_{\mathbf{k}} - \widehat{\mathbf{u}}_{\mathbf{k}}\phi_{\mathbf{k}}\|_3\|_T}{\|\|\sum_{\mathbf{k}\in\mathbf{K}}\widehat{\mathbf{u}}_{\mathbf{k}}\phi_{\mathbf{k}}\|_3\|_T}. \tag{22}$$

Due to turbulence the error will grow in time and eventually will become of the same order as the velocity field itself. To avoid this complication we will only look at statistical properties. We take the time average of the Fourier components before comparing the two velocity fields. The new discretization error δ is therefore defined as

$$\delta = \frac{[\sum_{\mathbf{k}\in\mathbf{K}}(\|\mathbf{u}_{\mathbf{k}}\|_T - \|\widehat{\mathbf{u}}_{\mathbf{k}}\|_T)^2]^{1/2}}{(\sum_{\mathbf{k}\in\mathbf{K}}\|\widehat{\mathbf{u}}_{\mathbf{k}}\|_T^2)^{1/2}}. \tag{23}$$

Note that this error is taken in the same way as the interpolation error; see relation (9). Next we use the fact that the energy spectrum for homogeneous isotropic turbulence is spherically symmetric as done before, which results in

$$\delta_{\text{iso}}^2 = \frac{\sum_{k=0}^{k_{\max}}k^2|\|\mathbf{u}_k\|_T - \|\widehat{\mathbf{u}}_k\|_T|^2}{\sum_{k=0}^{k_{\max}}k^2\|\widehat{\mathbf{u}}_k\|_T^2}. \tag{24}$$

This relation can be used to estimate the discretization error by the use of the energy spectrum.

TABLE I. Overview of the interpolation methods considered in this study. Note that for all methods the degree of the polynomial function is equal to $N-1$. n is the highest order of a polynomial function for which the interpolation is still exact [8].

Interpolation method	n	Order of continuity	FFT	Comment
Lagrange	$N-1$	0	1	for even N
		-1	1	for odd N
Spline	$N-2$	$(N-2)/2$	1	only even N
Hermite	$N-1$	1	8	only for $N \in 4\mathbb{N}$
B-spline	$N-1$	$N-2$	1	all N

TABLE II. Details of the DNS simulations of homogeneous isotropic turbulence. Three grids are used for comparison: a coarse, a fine, and a very well-resolved (reference) grid.

Grid	Number of grid points	$k_{\max}$	ν	$k_{\max}\eta$	Re_λ
Coarse	64	21	0.048	2.4	41
Fine	128	42	0.048	4.8	41
Reference	128	64	0.048	7.2	41

V. INTERPOLATION METHODS

The theory presented is tested on several different interpolation methods, namely Lagrange interpolation, spline interpolation, Hermite interpolation, and B-spline interpolation. In each spatial direction the methods investigated use N data points to construct a polynomial function of degree $N-1$ for the interpolation. For Hermite interpolation we use the method suggested by Choi *et al.* [13], who employ Hermite interpolation on multiple spatial points. For the B-spline interpolation the method of van Hinsberg *et al.* [8] is used.

In Table I all methods are listed with an overview of their main features. The order of continuity refers to the continuity C^n of the interpolation function. Furthermore, with FFT we refer to the number of fast Fourier transforms required for the interpolation. For Hermite interpolation also the derivatives are needed and this requirement increases the number of FFTs needed. In Fig. 1, $\gamma_k(k\Delta x)$, as from Eq. (20) is shown for the different interpolation methods, where Δx is the distance between the grid points.

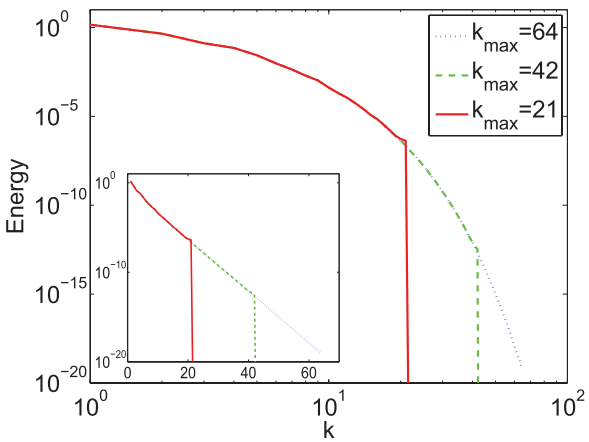

FIG. 2. (Color online) Energy spectra for different $k_{\max}$ in log-log scale. In the inset the same, but in log-lin scale.

TABLE III. Interpolation error for different methods calculated in different ways. Here $k_{\max}\eta = 2.4$ and $\delta = 5.03 \times 10^{-4}$.

Method	N	ϵ (1)	ϵ_{iso} (14) and (20)
Linear	2	5.44×10^{-3}	4.52×10^{-3}
Lagrange	4	3.67×10^{-4}	3.45×10^{-4}
Spline	4	4.39×10^{-4}	4.73×10^{-4}
B-spline	4	3.59×10^{-5}	3.99×10^{-5}
Hermite	4	3.82×10^{-5}	3.13×10^{-5}

VI. RESULTS

In this section we compare the interpolation methods. The discretization error is computed and compared with the interpolation error for all the interpolation methods. We estimate the errors by using the methods given by Eq. (24), for the discretization error, and by Eqs. (14) and (20) for the interpolation error. Subsequently, the methods are validated by investigating two different aspects: the error made in the location of the particles and the acceleration spectrum. Thanks to this quantitative comparison we are able to give a prediction of the optimal order N for the different interpolation methods as a function of $k_{\max}\eta$. Here η is the Kolmogorov length scale.

To compute the discretization error several simulations of homogeneous isotropic turbulence are performed with different $k_{\max}$; for details, see Table II. The energy spectra are reported in Fig. 2. Using relation (24), the discretization error can be computed. Next, also the interpolation error can be computed by directly using relation (1) or the approximate relations (14) and (20). Table III shows the interpolation error, calculated in the two different ways, to check the reliability of the approximation. The two proposed methods are found to be in agreement within 10%–20%, while the interpolation error changes over orders of magnitude for the different interpolation methods. The differences between the ways of estimating the interpolation error can be explained by statistical errors and approximations made in the theoretically derived error estimates.

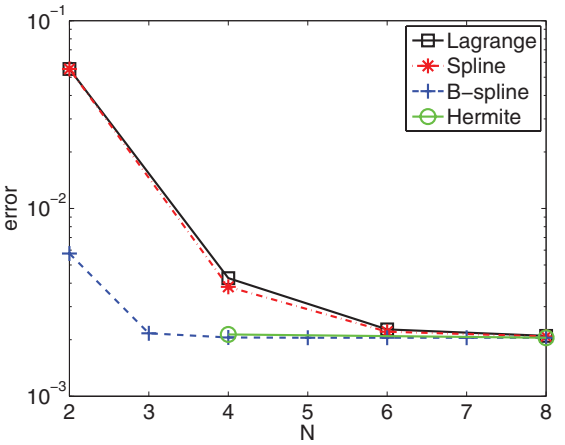

FIG. 4. (Color online) L^2-error at the position of a tracer after the Kolmogorov time scale ($t = 0.15$), with $k_{\max}\eta = 2.4$. The error is a combination of the interpolation and discretization error.

Next, to check the theory and the influence of the interpolation error, both errors in particle position and acceleration statistics are investigated. These errors are always a combination of the interpolation and the discretization error and how they evolve over time. In order to avoid unnecessary computations, still both errors should be of similar magnitude and therefore we can apply the theory. We start with observing the error in the position of the particle. The procedure is as follows: first, a family of tracers starting at one point is simulated with different interpolation methods; second, the reference tracer is simulated in a second simulation with double grid resolution keeping the initial condition and forcing the same. We started averaging over 50 particles, and in order to check statistical convergence and the eventual dependence on the initial condition, we repeated this for four different realizations of the flow field. After checking that the trend is the same the results shown here are averaged over the four realizations, for a total of 200 particles. The error in the particle

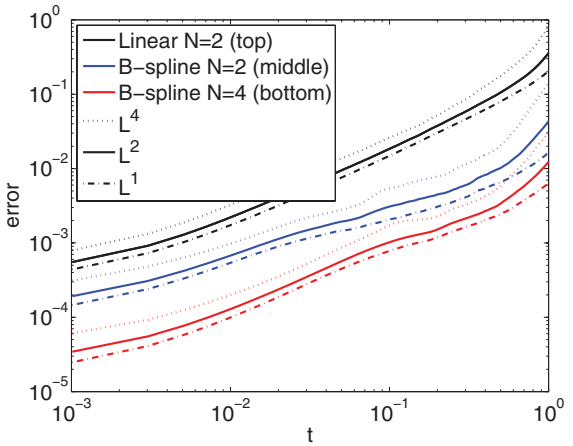

FIG. 3. (Color online) Error in the position of tracers for different interpolation methods and using different norms. The errors are plotted as a function of time and averaged over multiple particles.

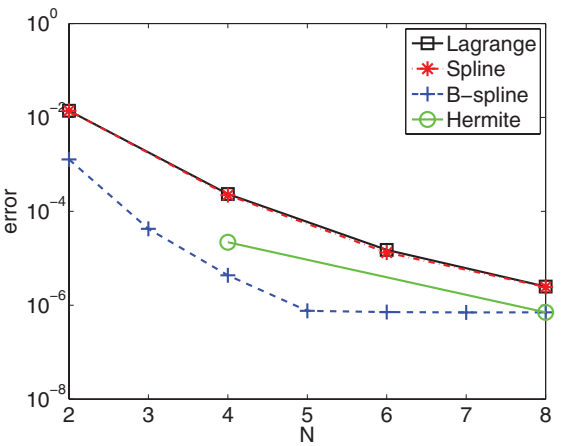

FIG. 5. (Color online) L^2-error at the position of a tracer after the Kolmogorov time scale, with $k_{\max}\eta = 4.8$. The error is a combination of the interpolation and discretization error.

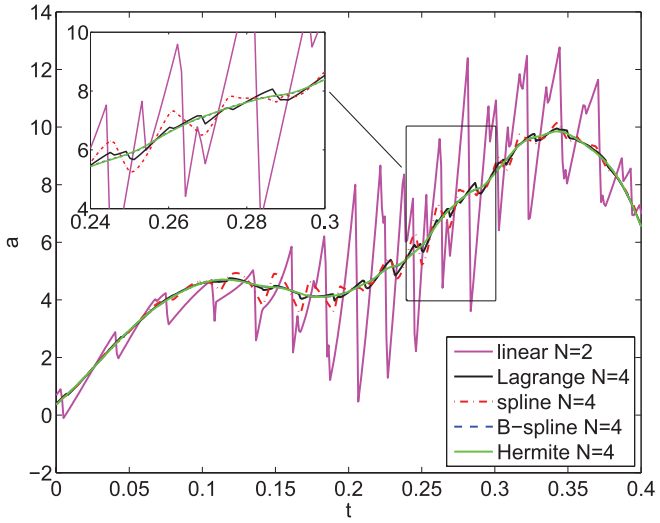

FIG. 6. (Color online) Particle acceleration of a fluid tracer, computed with different interpolation methods, where $k_{\max}\eta = 2.4$. The zigzagging is an artifact of the interpolation method.

position is plotted in Fig. 3 using different norms,

$$L^M = \|\mathbf{x}_p - \widetilde{\mathbf{x}}_p\|_M, \quad \|\mathbf{f}\|_M = \left(\sum_p |\mathbf{f}_p|^M\right)^{\frac{1}{M}}, \qquad (25)$$

where $\widetilde{\mathbf{x}}_p$ is the particle trajectory calculated by using interpolation methods and $\mathbf{x}_p$ is the exact particle trajectory, calculated using double grid resolution. In Fig. 3, one can see that even after one large eddy turnover time, $t = 1$, the influence of the interpolation error dominates over chaotic behavior of turbulence. At $t = 1$ the errors for the different methods are still clearly separated. Next, we consider the L^2-error after the Kolmogorov time scale ($t = 0.15$) for the different interpolation methods; see Fig. 4. In the following, we focus on the L^2-norm because this is the norm used in Secs. II and III. In Fig. 4 one can see that higher-order interpolations indeed become more accurate and that for high N no further accuracy is gained because the discretization error has become

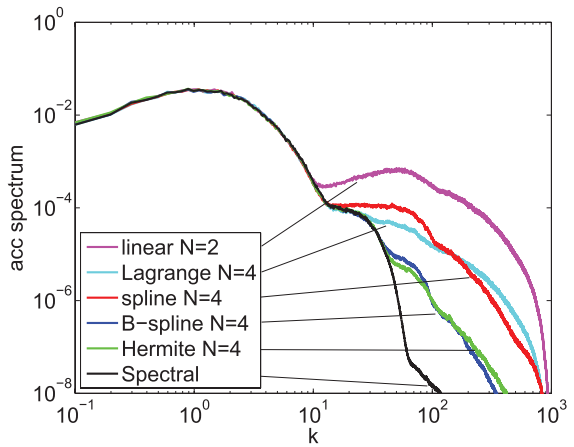

FIG. 7. (Color online) Particle acceleration spectrum, with $k_{\max}\eta = 2.4$. On the right side artificial energy is added due to both the interpolation and discretization error.

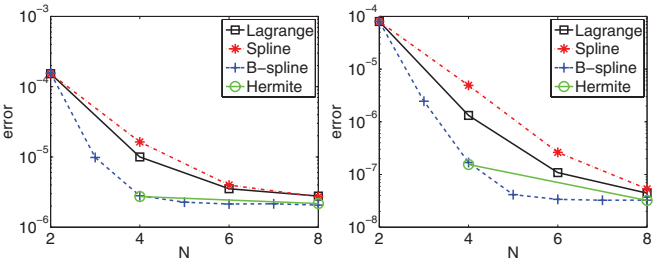

FIG. 8. (Color online) Error in the acceleration spectrum is plotted as a function of N, the order of the interpolation function. As error indication we employ the energy contained in the particle acceleration spectrum between wave numbers 20 and 3000. The error is a combination of both the interpolation and discretization error. (Left panel) $k_{\max}\eta = 2.4$. (Right panel) $k_{\max}\eta = 4.8$.

dominant over the interpolation error. This behavior is in agreement with the results in Table III. When increasing the resolution the discretization error becomes smaller and higher-order interpolation methods are needed to maintain the accuracy after interpolation; see Fig. 5.

In order to better show the influence of interpolation methods, we investigate the acceleration of the particle. Not only is the acceleration itself of great interest as a statistical quantity, see, for example, Ref. [3], but it is also needed to calculate the hydrodynamic forces in the Maxey-Riley equation. The acceleration signal of a generic particle as a function of time is shown in Fig. 6. The high-frequency oscillations are clearly nonphysical and with more accurate interpolation methods they disappear. To better quantify this effect, we analyze the acceleration spectrum of the particles. From Fig. 7 it can be seen that even the spectral interpolation shows a kink in the spectrum (around $k = 13$) due to the discretization error. For higher $k_{\max}\eta$ this kink is still observed, but at higher wave numbers. The energy content within the range of wave numbers between 20 and 3000 is computed and used as an error indication; see Fig. 8. Again the same behavior is found as in Figs. 4 and 5, as predicted by the theory.

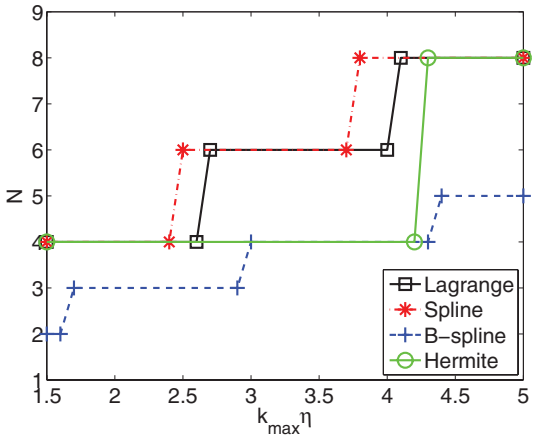

FIG. 9. (Color online) Optimal order N for the different interpolation methods with $k_{\max} = \frac{1}{3\Delta x}$. The optimal N is found by the criterium that the interpolation error is not allowed to exceed the discretization error.

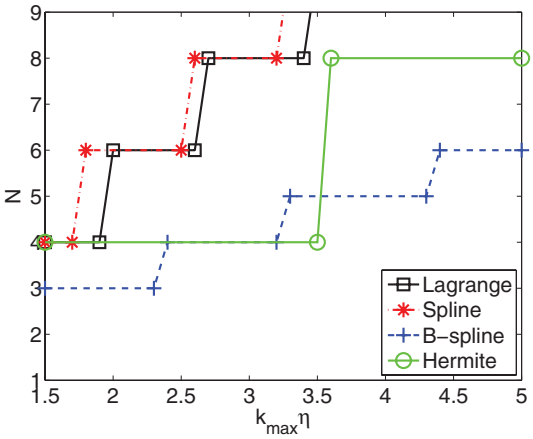

FIG. 10. (Color online) Optimal order N for the different interpolation methods, with $k_{max} = \frac{\sqrt{2}}{3\Delta x}$. The optimal N is found by the criterium that the interpolation error is not allowed to exceed the discretization error.

Now that the methods are validated for computing the interpolation error, the theory can be used to forecast which interpolation method is optimal for a given $k_{max}\eta$, independent of the Reynolds number. As increasing N of the interpolation method is much less time consuming than improving the resolution, the interpolation error is not allowed to exceed the discretization error. Using this criterium the optimal N can be found for a given $k_{max}\eta$ and interpolation method; see Fig. 9. In this simulation we did not allow for any aliasing of the nonlinear term; therefore, $k_{max} = \frac{1}{3\Delta x}$. In order to increase the accuracy, k_{max} can be increased allowing for some aliasing; see Fig. 10.

From Figs. 9 and 10 it can be seen that interpolation methods become more important when going to higher values of $k_{max}\eta$. Typical $k_{max}\eta$ values used are around 1.5, but studies have been performed with values up to 34 [24]. As the full Maxey-Riley equation also uses derivatives of the flow field the accuracy of the flow field should be increased, implying $k_{max}\eta \approx 3$ or higher. Here, B-spline interpolation is by far outperforming the other interpolation methods. The only interpolation method that is comparable is the Hermite interpolation; however, a drawback is that it can only be used for N a multiple of 4, thus limiting its flexibility. Furthermore, in order to employ Hermite interpolation also derivatives are needed making it computationally expensive (due to the need to evaluate many FFTs per derivative). To conclude, we found that B-spline interpolation is very suited for particle tracking simulations.

VII. CONCLUSIONS

We have introduced different practical methods for computing the error in the interpolation of the fluid velocity. First, we have introduced an accurate method that uses the full three-dimensional energy spectrum to estimate this error. Second, we introduced a practical method that only needs the one-dimensional energy spectrum to estimate the same error. These methods are validated by means of turbulent simulations and it is shown that they give accurate results.

Further we show the effect of the interpolation methods on both errors of particle positions and the acceleration spectrum. Particularly, the latter is important because the particle acceleration enters directly in the Maxey-Riley equation. The results for both the errors on particle positions and the acceleration spectrum are in agreement with the predictions of the theory.

Finally, we could provide a prediction for the optimal order of the different interpolation methods as a function of $k_{max}\eta$. In order to investigate the behavior of almost neutrally buoyant particles also derivatives of the flow field need to be accurately resolved, this implying values of $k_{max}\eta$ around 3 or higher. At these values of $k_{max}\eta$, B-spline interpolation performs much better than the other interpolation methods, implying less computational overhead.

ACKNOWLEDGMENTS

We thank B. J. H. van de Wiel for fruitful discussions. The authors gratefully acknowledge financial support from the Dutch Foundation for Fundamental Research on Matter (FOM) (Program 112 “Droplets in Turbulent Flow”). This work was sponsored by the Stichting Nationale Computerfaciliteiten (NCF) for the use of supercomputer facilities, with financial support from the Netherlands Organization for Scientific Research (NWO). The European COST Action MP0806 “Particles in Turbulence” is also acknowledged.

[1] P. K. Yeung and S. B. Pope, J. Comput. Phys. **79**, 373 (1988).
[2] K. D. Squires and J. K. Eaton, Phys. Fluids A **3**, 1169 (1991).
[3] F. Toschi and E. Bodenschatz, Annu. Rev. Fluid Mech. **41**, 375 (2009).
[4] L. Biferale, G. Boffetta, A. Celani, B. J. Devenish, A. Lanottea, and F. Toschi, Phys. Fluids **17**, 115101 (2005).
[5] R. Benzi, L. Biferale, R. Fisher, D. Q. Lamb, and F. Toschi, J. Fluid Mech. **653**, 221 (2010).
[6] F. Lekien and J. Marsden, Int. J. Numer. Method Eng. **63**, 455 (2005).
[7] E. Catmull and R. Rom, in *Computer Aided Geometric Design*, edited by R. E. Barnhill and R. F. Reisenfeld (Academic Press, New York, 1974), pp. 317–326.
[8] M. A. T. van Hinsberg, J. H. M. ten Thije Boonkkamp, F. Toschi, and H. J. H Clercx, SIAM J. Sci. Comput. **34**, B479 (2012).
[9] M. R. Maxey and J. J. Riley, Phys. Fluids **26**, 883 (1983).
[10] E. Loth, Prog. Energy Combust. Sci. **26**, 161 (2000).
[11] E. E. Michaelides, J. Fluids Eng. **125**, 209 (2003).
[12] M. A. T. van Hinsberg, J. H. M. ten Thije Boonkkamp, and H. J. H Clercx, J. Comput. Phys. **230**, 1465 (2011).
[13] J. Choi, K. Yeo, and C. Lee, Phys. Fluids **16**, 779 (2004).
[14] G. D. Reeves, R. D. Belian, and T. A. Fritz, J. Geophys. Res. **96**, 13997 (1991).
[15] F. Mackay, R. Marchand, and K. Kabin, J. Geophys. Res. **111**, A06208 (2006).

[16] T. M. Lehmann, C. Gönner, and K. Spitzer, IEEE Trans. Med. Imag. **18**, 1049 (1999).
[17] H. S. Hou and H. Andrews, IEEE Trans. Acoust., Speech and Signal Process. **26**, 508 (1978).
[18] H. Homann, J. Dreher, and R. Grauer, Comput. Phys. Commun. **177**, 560 (2007).
[19] C. Marchioli, V. Armenio, and A. Soldati, Comput. Fluids **36**, 1187 (2007).
[20] C. Marchioli, A. Soldati, J. G. M. Kuerten, B. Arcen, A. Tanière, G. Goldensoph, K. D. Squires, M. F. Cargnelutti, and L. M. Portela, Int. J. Multiphase Flow **34**, 879 (2008).
[21] G. B. Jacobs, D. A. Kopriva, and F. Mashayek, J. Comput. Appl. Math. **206**, 392 (2007).
[22] G. E. Karniadakis and J. S. Hesthaven, J. Eng. Math. **56**, 201 (2006).
[23] C. C. Lalescu, B. Teaca, and D. Carati, J. Comput. Phys. **229**, 5862 (2010).
[24] J. Schumacher, K. R. Sreenivasan, and P. K. Yeung, J. Fluid Mech. **531**, 113 (2005).